

## Article

# Validation of Solid-State LiDAR Measurement System for Ballast Geometry Monitoring in Rail Tracks

Enrique Aldao <sup>1</sup>, Higinio González-Jorge <sup>1,\*</sup>, Luis Miguel González-deSantos <sup>1</sup>, Gabriel Fontenla-Carrera <sup>1</sup>  
and Joaquin Martínez-Sánchez <sup>2</sup>

<sup>1</sup> Research Institute of Physics and Aerospace Science, University of Vigo, Campus Ourense, 32004 Ourense, Spain

<sup>2</sup> CINTECX, Applied Geotechnology Group, University of Vigo, 36310 Vigo, Spain

\* Correspondence: higinio@uvigo.gal

**Abstract:** The inspection and maintenance of track ballast are fundamental tasks for the preservation of the condition of railway networks. This work presents an application based on a low-cost solid-state LiDAR system, which allows the user to accurately measure the ballast geometry from a mobile inspection trolley or draisine. The solid-state LiDAR system, the LiVOX Avia, was validated on a test track through comparison with a traditional static LiDAR system, the Faro Focus 3D. The results show a standard deviation of around 6 mm for the solid-state LiDAR system. The LiVOX system also provides the capability to measure the ballast digital elevation model and profiles. The LiVOX results are in agreement with those obtained from the Faro Focus. The results demonstrate that the LiVOX system can sufficiently measure even the displacement of a single layer of ballast stones typically between 2.5 cm and 5 cm. The data provided can be easily digitalized using image processing tools and integrated into geographic information systems for infrastructure management.

**Keywords:** railway maintenance; solid-state LiDAR; ballast; metrology



**Citation:** Aldao, E.; González-Jorge, H.; González-deSantos, L.M.; Fontenla-Carrera, G.; Martínez-Sánchez, J. Validation of Solid-State LiDAR Measurement System for Ballast Geometry Monitoring in Rail Tracks. *Infrastructures* **2023**, *8*, 63. <https://doi.org/10.3390/infrastructures8040063>

Academic Editors: Chunxu Qu, Jinhe Gao, Rui Zhang, Ziguang Jia and Jiaxiang Li

Received: 4 March 2023

Revised: 16 March 2023

Accepted: 22 March 2023

Published: 23 March 2023



**Copyright:** © 2023 by the authors. Licensee MDPI, Basel, Switzerland. This article is an open access article distributed under the terms and conditions of the Creative Commons Attribution (CC BY) license (<https://creativecommons.org/licenses/by/4.0/>).

## 1. Introduction

Railways have been the key to the socioeconomic development of societies around the world since the first locomotive developments carried out by Stephenson [1] over two centuries ago. At present, where sustainability and the fight against climate change are very important matters, railways are shown to be one of the least polluting means of transport due to their easy electrification. This, together with the deployment of high-speed rail networks competing with aviation in the medium distance, undoubtedly makes railways one of the means of transport of the future [2,3].

Infrastructure management companies need to systematically carry out different maintenance works to ensure that railroad networks are in good condition for operations [4–6]. These works range from the inspection of different track elements such as the rails, ballast, tightening bolts or sleepers to the management of the different repair works necessary to keep the infrastructure in operation under safety conditions [7–9]. Although many inspections are still performed visually by human operators, the current trend is to automate such work, through on-board sensors on railway locomotives, draisines or track trolleys, and artificial intelligence techniques. The sensors used are of different types such as imaging or acoustic sensors [10,11].

Ballast is one of the main elements of railroads. It is responsible for transferring the loads onto the ground and must have a certain elasticity and prevent transverse and longitudinal movements of the track. It also prevents vegetation from growing around the platform, reduces the sound of trains and improves rainwater drainage to prevent deterioration. For ballast to work properly, it is essential to select the right type of material and the right grain size. The importance of railway ballast should not be underestimated; it is a component that can make a difference in the performance of railways [12].

Due to the loads and vibrations to which ballast is subjected by the passage of trains, it is necessary to periodically conduct maintenance operations that focus on the profiling and dynamic stabilization of the ballast [13–15]. Track profiling is a maintenance operation that aims to bring the profile of the track to the proper shape by distributing the ballast. The profiling operations are carried out by means of a profiling machine containing a series of lateral plows, which are used to collect ballast that has escaped from the railway due to the actions of trains. This machine usually works together with a tamping machine, accompanying it in all the work it performs. Since the average performance of a profiling machine is much higher than that of any tamping machine [16], the former usually works better ahead of the latter, in order to obtain the optimal joint performance of the two machines. The dynamic stabilization operations of a track consist of subjecting it to a horizontal vibration and a static vertical load simultaneously, in such a way as to promote the spatial redistribution of the aggregates that make up the ballast and a reduction in voids in the ballast. By filling the existing voids in the apparent volume of ballast, a greater compactness is achieved, therefore providing an improvement in the stability of the infrastructure in the face of the traffic stresses imposed on it. The dynamic stabilization of a track is carried out by means of specific machinery, including two elements located under the main frame. Each of these elements is composed of four retaining rollers inside the rail head, two turntables on the outside of the rail head and a vibrating group. The two vibrating groups are synchronized and transmit horizontal vibrations to the track through the rollers holding the rail head. The total percussion force reaches hundreds of kN. The approximate values of the vibration frequency and vertical load applied to each rail are around 30 Hz and 12 Tons, respectively.

Accurate rail infrastructure maintenance management must be accompanied by accurate inspection systems, where the evaluation of the ballast geometry/profile is a key aspect. Typically, photogrammetry and LiDAR systems are used for this purpose.

Zhang et al. (2016) reported a prototype of a non-intrusive track ballast inspection system based on the digital camera of a smartphone and photogrammetric algorithms [17]. The analysis was based on cloud-based photogrammetry processing. Paixao et al. (2018) presented a methodology to evaluate the ballast structure using a cost-effective photogrammetric 3D reconstruction. They produced digital models that allowed for automated particle geometry analysis [18]. Paixao et al. (2022) presented an evaluation of ballast particle degradation using close-range photogrammetry. Using this technique, they took into consideration the morphology of the ballast (e.g., shape, angularity and surface texture) [19].

LiDAR systems have shown great usability in infrastructure inspection in the last decade, both in the road [20] and rail domains [21]. Regarding the inspection of railroad track ballast, Zarembski et al. (2014) introduced inspection technologies such as LiDAR for the measurement of the ballast profile, ground-penetrating radar for the inspection of ballast depth deficiency, and other related inspection technologies [22]. Zarembski et al. (2017) used a rail-mounted LiDAR-based ballast profile measurement system to obtain the geometry, profiles and missing ballast volume of a track section. They used data-intensive algorithms in order to effectively analyze over 100,000 segments of track representing more than 1500 km [23]. Sun et al. (2020) used LiDAR for the full-section inspection of tunnels (e.g., section extraction, structural deformation and ballast analysis). They obtained a spatial resolution of 2 mm in the ballast part. The system includes human–computer interaction to extract and label damage in the infrastructure or appurtenances and support the generation of thematic damage maps [24]. Nie et al. (2021) reported a study of ballast degradation simulating a typical freight train with an average speed of 120 km/h and 30-ton capacity using a cyclic loading test. They used a LiDAR system for the volumetric parametrization of the results. The overall experimental results showed that ballast degradation was more profound in the early stage of service [25].

Traditional LiDAR systems based on a laser scanner show advantageous features such as a high accuracy, but they are expensive. They also have moving parts that are sometimes

fragile when operating in harsh environments, such as the inspection of a railway track, especially when used at high speeds. This opens the interest in testing the applicability of solid-state LiDAR-based systems, which are shown to be more robust as they have no moving parts and are also much cheaper. The solid-state sensor tested in this work was a LiVOX Avia. This sensor is typically used in applications such as aerial drones, although it can also be successfully used in ground-based systems [26,27]. Thus far, this sensor has been used mainly in applications such as forestry and road management, but there are still no known applications in the railway field, specifically in the measurement of ballast. Therefore, the study presented here should be of interest to the field of railway maintenance.

The aim of this work was to present a verification of the metrological performance of a LiVOX system mounted on an experimental track trolley. To this end, benchmarking with a highly tested Faro Focus 3D scanner was conducted. This study was oriented to verifying the geometrical condition of the ballast and compared the accuracy of both systems in obtaining profiles of the track transversal section and measuring the digital elevation model. The precision of the system was also determined. This manuscript is structured in the following sections: Section 2 presents the materials and methods; Section 3 presents the results and discussion; and Section 4 presents the conclusions.

## 2. Materials and Methods

This section presents the different materials and methodologies used in this work. Among the materials, we used a track section for the tests, and a track trolley to carry the on-board inspection sensors, namely, the LiDAR LiVOX under study and the Faro Focus 3D system used as a measurement standard. The methods included the different tests conducted for the verification of the LiVOX metrological parameters, for obtaining both the ballast profiles and the digital elevation model.

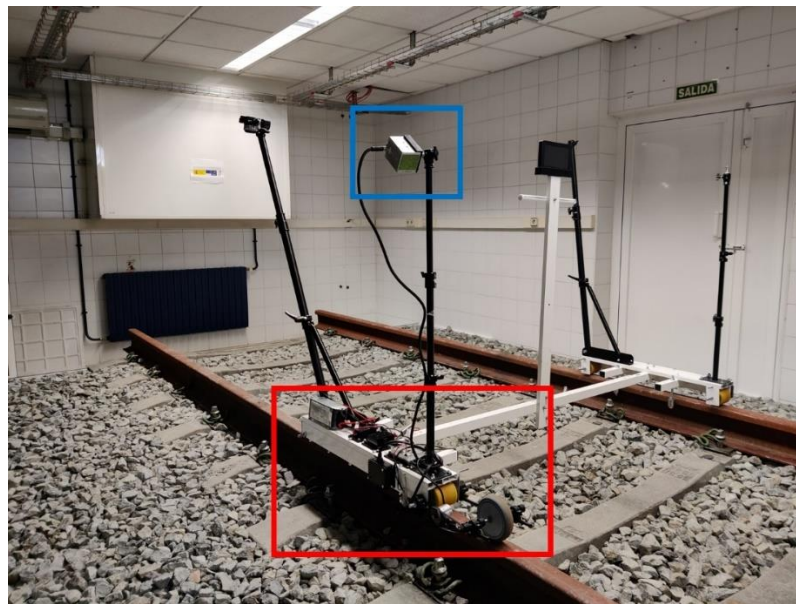
### 2.1. Materials

Figure 1 shows the main infrastructure used for testing the solid-state LiDAR system in the measurement of the ballast geometry. The infrastructure consists of a section of track comprising a steel rail, concrete sleepers and ballast as structural support. It is located in the basement of the Martínez Risco Building, sited in the Ourense Campus of the University of Vigo (Spain). The track section was installed by the construction company COPASA [28], as part of the works being carried out in the RIIM (Railway Inspection and Information Model) project. It is an Iberian gauge track (width: 1.668 mm) with a total length of five meters [29].

The different tests performed with the solid-state LiDAR sensors in motion were conducted by means of a track trolley that was designed and developed for this purpose. The system under study is a dismountable and modular system built in aluminum, which allows for testing in indoor facilities and also on a real track. Figure 1 shows the position of the LiVOX LiDAR system in the trolley (blue rectangle) and the navigation system (red rectangle) based mainly on odometry (Sick HTL DBS36). Thus, each frame acquired with the LiDAR system was synchronized with the movement of the trolley and monitored by the odometer, and a complete point cloud of the study area was calculated. In this case, due to the fact that the data collection was performed indoors on a small track section, it was decided not to integrate greater complexity into the acquisition system with satellite positioning sensors (GNSS) or inertial guidance (IMU).

The technical specifications of the LiVOX Avia system (Table 1) include a pulse repetition rate of up to 240,000 points/s, a scanning rate of 0.1 s, a detection range between 190 m (10% reflectivity) and 320 m (80% reflectivity), a field of view in the repetitive scanning pattern mode of  $70.4^\circ$  (horizontal)  $\times$   $4.5^\circ$  (vertical), a distance random error of 2 cm ( $1\sigma$ ), an angular random error of  $0.05^\circ$  ( $1\sigma$ ), a beam divergence of  $0.03^\circ$  (horizontal)  $\times$   $0.28^\circ$  (vertical) and a laser wavelength of 905 nm [30]. The data provided by the LiVOX system

and the synchronization data from the odometer were processed by a Raspberry Pi 4B computer and saved in a USB 3.0 flash drive.



**Figure 1.** Infrastructure used for the validation of the solid-state LiDAR system. The LiVOX Avia (blue) and navigation system (red) are highlighted.

**Table 1.** Technical specifications of the LiVOX Avia and Faro Focus 3D.

| Feature                 | LiVOX Avia   | Faro Focus 3D                              |
|-------------------------|--|--|
| Pulse repetition rate   | 240,000 points/s                                     | 976,000 points/s                           |
| Scanning rate           | 10 Hz  | 97 Hz                                      |
| Maximum detection range | 320 m (80% reflectivity)<br>190 m (10% reflectivity) | 153.49 m                                   |
| Field of view           | 70.4° (H) × 4.5° (V)                                 | 305° (H) × 360° (V)                        |
| Laser wavelength        | 905 nm   | 905 nm                                     |
| Range precision         | 2 cm (1 $\sigma$ )                                   | 1.2 mm (10 m range)<br>2.2 mm (25 m range) |
| Angular precision       | 0.05°  | 0.009°                                     |
| Beam divergence         | 0.03° (H) × 0.28° (V)                                | 0.01°                                      |
| Data storage            | USB 3.0 flash drive                                  | SD card                                    |

The Faro Focus 3D is a static LiDAR system (tripod-based), which was used as a standard instrument for the validation of the LiVOX data (Table 1). In terms of precision and accuracy, the Faro’s characteristics are far superior to those of the LiVOX, making it a valid system for the purpose of acting as a reference sensor. It has a pulse repetition rate of up to 976,000 points/s, an unambiguity range of 153.49 m, a recommended measurement range between 0.6 m and 120 m, a ranging error of 2 mm at 10 m and 25 m, ranging noise of 1.2 mm at 10 m and 2.2 mm at 25 m, a field of view of 305° (vertical) × 360° (horizontal), an angular precision of 0.009° (both vertical and horizontal), a beam divergence of 0.01° and a laser wavelength of 905 nm [31]. The data provided by the Faro Focus 3D were saved in an SD card.

## 2.2. Methods

Three methods were developed for the metrological evaluation of the ballast geometric measurements with the solid-state LiDAR sensor LiVOX Avia: standard deviation of measurements, evaluation of ballast profiles and evaluation of the digital elevation model of the ballast.

### 2.2.1. Standard Deviation of Measurements

The evaluation of the standard deviation of the measurements was performed using a flat surface as a reference—in this case, six tiles located in the basement of the Martinez Risco Building where the test track section is located (Figure 2). Six LiDAR scans of these tiles were performed using the solid-state LiDAR system under study, the LiVOX Avia, and the Faro Focus 3D as a reference system. The point clouds obtained were loaded into the Cloud Compare software for data processing and analysis [32]. Data processing consisted of the segmentation of the area under study and plane fitting using the least squares method to calculate the root mean square error, indicative of the standard deviation of the measurements. The different results obtained by the LiVOX and Faro Focus LiDAR systems were compared [33].

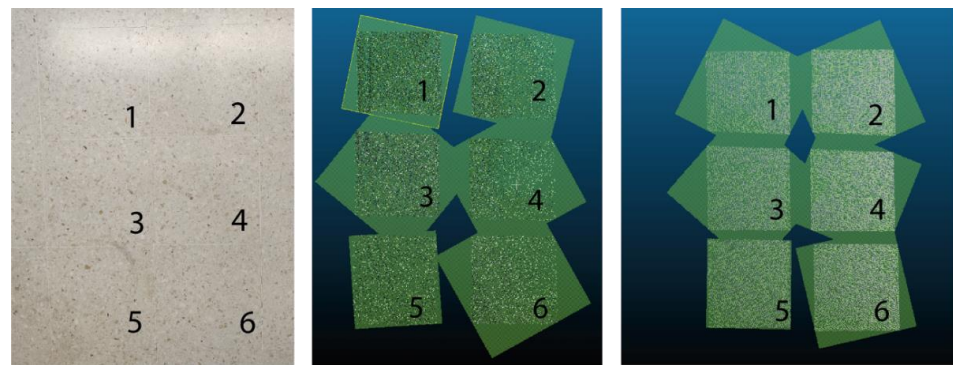


**Figure 2.** Standard deviation measurements: tiles (left), LiVOX Avia point cloud and plane fitting (center) and Faro Focus 3D point cloud and plane fitting (right).

### 2.2.2. Digital Elevation Model and Ballast Profiles

It is understood that the interest of a system such as LiVOX comes from its capacity to perform geometric measurements of ballast, which, for example, indicate the displacement, loss of material or subsidence of the foundation. Therefore, the studies carried out were based on the following methodology:

First, scanning of the track was carried out using both systems, i.e., the LiVOX system mounted on the track trolley with the encoder, and the Faro Focus 3D.

The data acquisition with the Faro Focus 3D was carried out by means of four scanning stations at the corners of the track. This was followed by a manual coarse registration process and precision registration based on the iterative closest point (ICP) algorithm using Cloud Compare [34]. This ensured that there were no occluded areas with missing data. Once the four-point clouds of the Focus 3D LiDAR system were registered, a registration was also performed with the LiVOX data, to ensure that the data from the two scanners used the same coordinate system. Figure 3 shows the LiDAR results. It should be noted that the LiVOX system covered half of the track. To perform a complete scan of the track, two systems working synchronously would be needed.

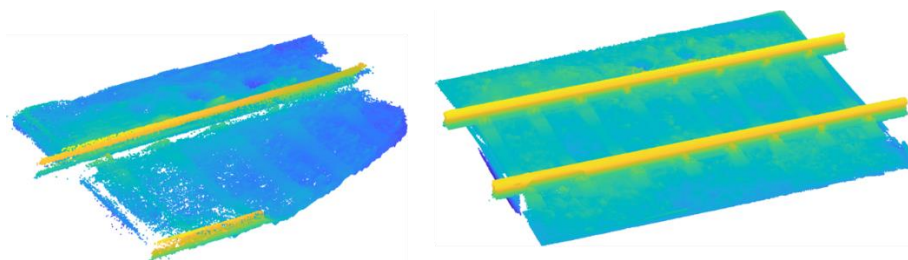


**Figure 3.** LiDAR data: LiVOX Avia (left) and Faro Focus 3D (right).

Three holes of different dimensions were then dug in the ballast (Figure 4), and the scanning process was repeated with both sensors. In this way, the ballast geometry can be compared before and after acting on it, and it can be determined whether the LiVOX system has sufficient sensitivity to detect geometrical changes in the material.



**Figure 4.** Holes dug in the ballast (marked in green).

Finally, the evaluation of the results was carried out by means of two procedures. On the one hand, three ballast profiles were measured in the area of the holes. These profiles were analyzed for the two LiDAR systems, both before and after the holes were dug. On the other hand, a rasterization of the point clouds was performed for each scanner, before and after digging the holes, so that a digital elevation model (DEM) with centimeter resolution was generated [35]. Afterwards, the difference between the two digital elevation models, before and after digging the holes, was determined pixel by pixel to evaluate the volumetric change.

### 3. Results

Figure 5 shows the comparison of the root mean square error (RMSE) obtained using the LiVOX and Faro Focus scanners. The data were obtained following the methods described in Section 2.2.1. The RMSE appeared to be very stable in all systems under study for the six measured tiles. This demonstrates the high reproducibility and stability of the measurements. In all cases, the Faro Focus 3D obtained a value lower than 1 mm, while the LiVOX Avia obtained values between 5 mm and 7 mm. This characteristic, which is indicative of system noise/precision and should be differentiated from the distance measurement error, which is more indicative of the accuracy, is not specified in the system datasheet and motivated the realization of this test [30]. It can be observed that, although the

standard deviation obtained by the LiVOX was about five times higher than that obtained by the Faro, its measurements were below 1 cm, which should allow for measuring the displacement of at least one layer of ballast stones, which usually have a diameter between 2.5 cm and 5 cm [36]. The displacement of this layer would not produce a structural problem in the ballast, but it would set a geometric limit on the sensitivity of the solid-state LiDAR system.

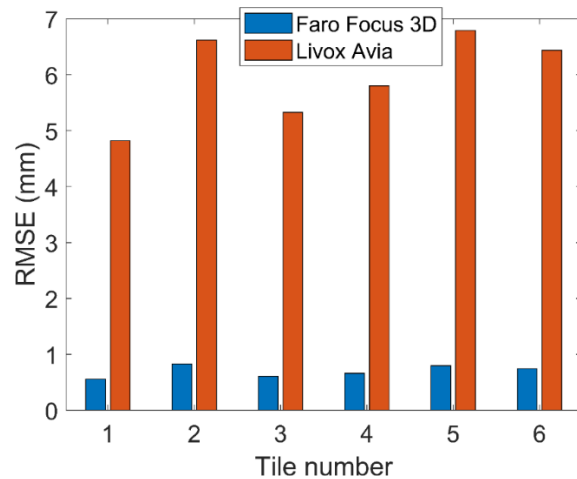


**Figure 5.** Benchmarking of the LiDAR systems’ standard deviation. RMSE indicates the root mean square error of the point cloud fitting to a plane using least squares fitting.

Figure 6 shows the cloud-to-cloud distance between the Faro Focus 3D point cloud and the LiVOX Avia. This result was obtained using the Cloud Compare tool. The algorithm first computed approximate distances, which were used internally to automatically set the best octree level at which to perform the real distance computation. In this case, the reference cloud was the Faro Focus 3D data from the track section, while the LiVOX Avia cloud was the cloud under analysis (see Figure 3). The software provided a statistic of the comparison between the point clouds, where 85% of the points from the LiVOX Avia were placed at a distance shorter than 10 mm. These results are consistent with those depicted in Figure 5, where the LiVOX Avia shows a standard deviation below 7 mm.

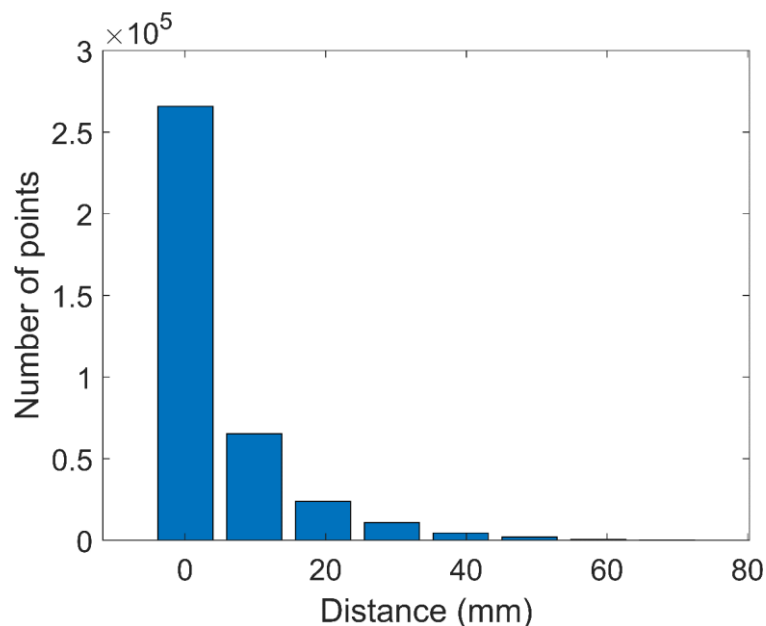


**Figure 6.** Cloud-to-cloud distance between the Faro Focus 3D and the LiVOX Avia.

Figure 7 depicts a digital elevation model after the three holes were dug. It also indicates the profiles under study, which are shown in Figure 8. The profiles reveal the comparison between the LiVOX Avia and the Faro Focus 3D, before and after digging the holes. Firstly, it can be observed that the profiles obtained by the LiVOX correlate accurately with those obtained by the Faro Focus, both before and after the ballast movements. It is also observed that the LiVOX system was able to detect the holes dug, even in profile 1, which had a shallower depth. In both cases, it also effectively detected the zone where the small stones that were removed from the hole were moved. In all the figures, after the holes were dug, from 80 cm on the X axis, an increment in the ballast profile can be observed, which coincides with the zone that acted as the stone deposit.

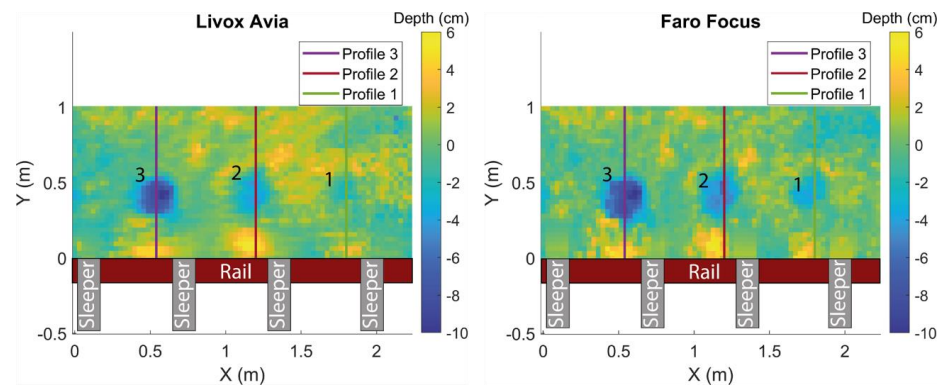


Figure 7. Digital elevation models of the ballast and locations of the profiles of the LiVOX Avia (left) and Faro Focus 3D (right) under study.

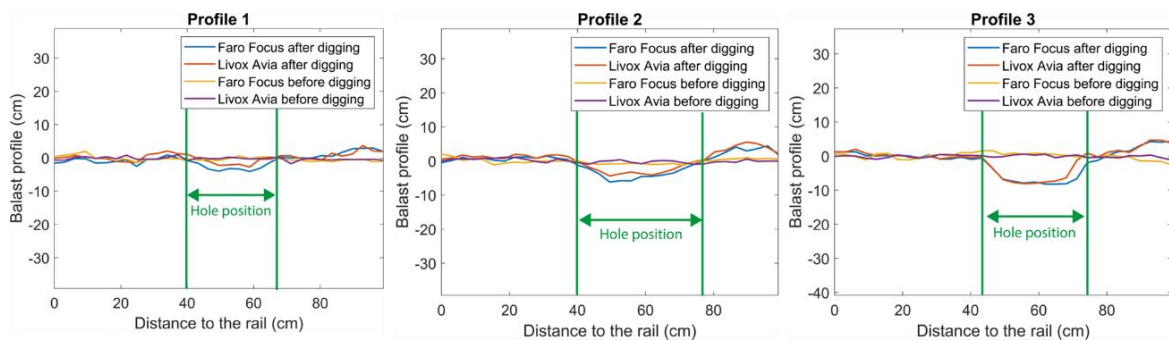
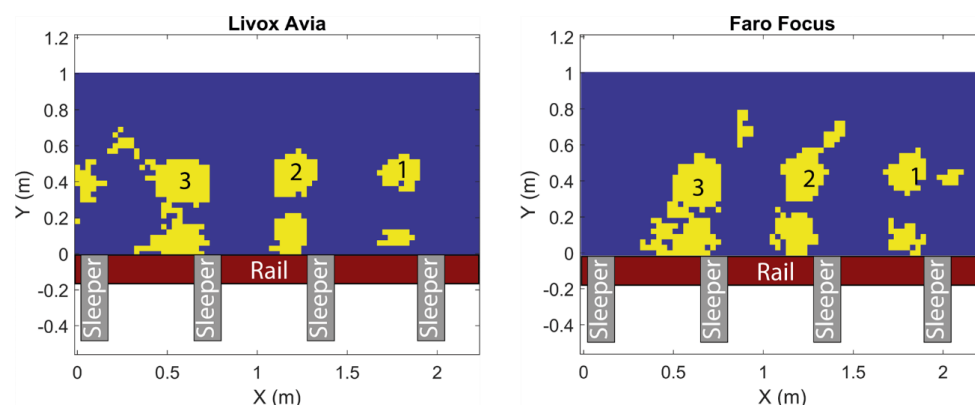


Figure 8. Ballast profiles comparing the results of the LiVOX Avia and Faro Focus 3D, before and after digging the holes.

Figure 9 shows binarized images of the ballast indicating the areas where the holes were dug. These images were generated by calculating the difference pixel by pixel between the DEMs of the ballast before and after digging the holes, for each scanner. Once the DEM difference was evaluated, the threshold for the binarization was estimated as 18 mm (3-sigma standard deviation to cover 99% of the results). Thus, changes in the ballast higher than 18 mm are represented by yellow, and changes lower than 18 mm are represented by blue. Some salt-and-pepper-type noise is shown that can be largely filtered out using image morphology operations, as shown in the figure, with most of the noise already removed. The purpose of presenting the results in this format is to show how data processing could be automated using computer vision techniques and generate an alert for infrastructure maintenance operations. In addition, spatial coordinates can be assigned to the image for the generation of orthoimages that could be integrated into geographic information systems and infrastructure management.



**Figure 9.** Binary images indicating the ballast displacements and holes: LiVOX Avia (left) and Faro Focus 3D (right).

#### 4. Conclusions

This work shows the application of a relatively new technology, namely, low-cost solid-state LiDAR systems, with the ability to be mounted on mobile inspection trolleys or draisines, for monitoring the geometry of railroad track ballast.

Solid-state LiDAR technology exhibits a lower precision than static LiDAR systems: in the comparison of an Avia LiVOX system versus a Faro Focus 3D system, a 6 mm standard deviation was obtained by the former versus less than 1 mm for the latter. However, this precision is sufficient to detect movements of only one ballast layer, whose stones have typical diameters between 2.5 cm and 5 cm. Although these movements are not usually representative from a structural point of view, they determine the sensitivity limit of the system.

The data obtained can be easily processed automatically, using different software tools. In this case, Cloud Compare software was used because the test section was a track of only 5 m, but more complex ad hoc algorithms can be developed to automate the processing.

Three holes of different depths were generated in the ballast and evaluated with the two LiDAR systems. Digital elevation models of the ballast before and after the holes were dug and the corresponding profiles were obtained. It was observed that the LiVOX system reproduced the data obtained with the Faro Focus system, even in the shallowest hole.

Finally, simple image processing was performed. For this, the difference between the digital elevation models obtained by the two scanners, before and after digging the holes, was evaluated. Then, a binarization of the results was performed using three times the standard deviation of the LiVOX Avia system as the threshold. The final image was treated using mathematical morphology techniques to eliminate salt and pepper noise. In the binarized image, it was possible to simply observe the area where the holes were dug, and even the area where the stones removed from the holes were deposited. These results can be easily integrated into geographic information systems used for infrastructure management and could contribute to the scalability of the technology.

Solid-state LiDAR systems could be used to inspect other railway elements such as the tunnel clearance or the position of the catenaries, simply by changing the orientation of the LiDAR system on the track trolley. Future trends will include the integration of solid-state LiDAR systems with accurate navigation technology (GNSS/IMU) to provide positioning and attitude in outdoor inspections and increase the speed and range of the inspections. In addition, it will also be important to synchronously use LiDAR systems and digital cameras to simultaneously monitor other track defects such as cracks in concrete sleepers or the condition of fastening clips. Solid-state LiDAR technology shows its applicability in the railway sector, although it could also be exploited in other fields of transport engineering, provided that the deformations to be measured are within the accuracy range of the system.

**Author Contributions:** Conceptualization, E.A., J.M.-S., L.M.G.-d. and H.G.-J.; Investigation, E.A. and H.G.-J.; Methodology, E.A., G.F.-C., L.M.G.-d. and H.G.-J.; Software, E.A. and J.M.-S.; Supervision, L.M.G.-d. and H.G.-J.; Writing—original draft, H.G.-J. and E.A.; Writing—review and editing, L.M.G.-d., G.F.-C. and J.M.-S. All authors have read and agreed to the published version of the manuscript.

**Funding:** E.A. is funded by the Spanish Ministry of Universities (grant ref: FPU21/01176). L.M.G.-d. is funded by the Recovery, Transformation and Resilience Plan of the European Union—Next GenerationEU (University of Vigo grant ref. 585507). Grant PLEC2021-007940 is funded by MCIN/AEI/10.13039/501100011033 and by the European Union NextGenerationEU/PRTR.

**Acknowledgments:** COPASA participated in the development of this work by providing support and resources to obtain the experimental data. It also collaborated in the definition of inspection system requirements, and its experience was essential for the development of the experiments.

**Conflicts of Interest:** The authors declare no conflict of interest.

## References

1. Cavendish, R. George Stephenson's first steam locomotive. *Hist. Today* **2014**, *64*, 7. Available online: <https://www.historytoday.com/archive/george-stephensons-first-steam-locomotive> (accessed on 26 December 2022).
2. Guo, X.; Sun, W.; Yao, S.; Zheng, S. Does high-speed railway reduce air pollution along highways? Evidence from China. *Transp. Res. Part D: Transp. Environ.* **2020**, *89*, 102607. [\[CrossRef\]](#)
3. Lalive, R.; Luechinger, S.; Schmutzler, A. Does expanding regional train service reduce air pollution? *J. Environ. Econ. Manag.* **2018**, *92*, 744–764. [\[CrossRef\]](#)
4. Zhu, L.; Yu, F.R.; Wang, Y.; Ning, B.; Tang, T. Big data analytics in intelligent transportation systems: A survey. *IEEE Trans. Intell. Transp. Syst.* **2019**, *20*, 383–398. [\[CrossRef\]](#)
5. Papaalias, N.P.; Roberts, C.; Davis, C.L. A review on non-destructive evaluation of rails: State-of-the-art and future development. *Proc. Inst. Mech. Eng. Part F J. Rail Rapid Transit.* **2008**, *222*, 367–384. [\[CrossRef\]](#)
6. Sainz-Aja, A.J.; Ferreño, D.; Pombo, J.; Carrascal, I.A.; Casado, J.; Diego, S.; Castro, J. Parametric analysis of railway infrastructure for improved performance and lower life-cycle costs using machine learning techniques. *Adv. Eng. Softw.* **2023**, *175*, 103357. [\[CrossRef\]](#)
7. Cannon, D.F.; Edell, K.O.; Grassie, S.L.; Sawley, K. Rail defects: An overview. *Fatigue Fract. Eng. Mater. Struct.* **2003**, *26*, 865–886. [\[CrossRef\]](#)
8. Popov, K.; De Bold, R.; Chai, H.K.; Forde, M.C.; Ho, C.L.; Hyslip, J.P.; Kashani, H.F.; Long, P.; Hsu, S.S. Big-data driven assessment of railway track maintenance efficiency using artificial neural networks. *Constr. Build. Mater.* **2022**, *349*, 128786. [\[CrossRef\]](#)
9. Luo, X.; Haya, H.; Inaba, T.; Shiotani, T.; Nakanishi, Y. Damage evaluation of railway structures by using train-induced AE. *Constr. Build. Mater.* **2004**, *18*, 215–223. [\[CrossRef\]](#)
10. Xin Wang, X.L.; Todd, L.E. Relationship between track geometry defect occurrence and substructure condition: A case study on one passenger railroad in the United States. *Constr. Build. Mater.* **2023**, *365*, 130066. [\[CrossRef\]](#)
11. Chen, L.; Chen, W.; Wang, L.; Zhai, C.; Hu, X.; Sun, L.; Tian, Y.; Huang, X.; Jiang, L. Convolutional neural networks (CNNs)-based multi-category damage detection and recognition of high-speed rail (HSR) reinforced concrete (RC) bridges using test images. *Constr. Build. Mater.* **2023**, *276*, 115306. [\[CrossRef\]](#)
12. Guo, Y.; Xie, J.; Fan, Z.; Markine, V.; Connolly, D.P.; Jing, G. Railway ballast material selection and evaluation: A review. *Constr. Build. Mater.* **2022**, *344*, 128218. [\[CrossRef\]](#)
13. Xiaio, H.; Fang, J.; Chi, Y.; Zhang, Z.; Ma, J.; Nadakatti, M.M.; Wang, X. Discrete element analysis of the effect of manual tamping operation on the manual tamping operation on the mechanical properties of ballast bed. *Constr. Build. Mater.* **2022**, *361*, 129557. [\[CrossRef\]](#)
14. Prescott, D.; Andrews, J. A track ballast maintenance and inspection model for a rail network. *Proc. Inst. Mech. Eng. Part O J. Risk Reliab.* **2013**, *227*, 251–266. [\[CrossRef\]](#)
15. Prasad, K.V.S.; Hussaini, S.K.K. Review of different stabilization techniques adapted in ballasted tracks. *Constr. Build. Mater.* **2022**, *340*, 127747. [\[CrossRef\]](#)
16. Guo, Y.; Markine, V.; Jing, G. Review of ballast track tramping: Mechanism, challenges and solutions. *Constr. Build. Mater.* **2021**, *300*, 123940. [\[CrossRef\]](#)
17. Zhang, B.; Lee, S.J.; Qian, Y.; Tutumluer, E.; Bhattacharya, S. A smartphone-based image analysis technique for ballast aggregates. In Proceedings of the International Conference on Transportation and Development, Houston, TX, USA, 26–29 June 2016; pp. 623–630. [\[CrossRef\]](#)
18. Paixao, A.; Resende, R.; Fortunato, E. Photogrammetry for digital reconstruction of railway ballast particles. A cost-efficient method. *Constr. Build. Mater.* **2018**, *191*, 963–976. [\[CrossRef\]](#)
19. Paixao, A.; Afonso, C.; Delgado, B.; Fortunato, E. Evaluation of ballast particle degradation under micro-deval testing using photogrammetry. *Lect. Notes Civ. Eng.* **2022**, *165*, 113–124. [\[CrossRef\]](#)

20. Díaz-Vilariño, L.; González-Jorge, H.; Bueno, M.; Arias, P.; Puente, I. Automatic classification of urban pavements using mobile LiDAR data and roughness descriptors. *Constr. Build. Mater.* **2016**, *102*, 208–215. [CrossRef]
21. Sánchez-Rodríguez, A.; Riveiro, B.; Soilán, M.; González-deSantos, L.M. Automated detection and decomposition of railway tunnels from mobile laser scanning datasets. *Autom. Constr.* **2018**, *96*, 171–179. [CrossRef]
22. Zarembski, A.M.; Grissom, G.T.; Euston, T.L. On the use of ballast inspection technology for the management of track substructure. *Transp. Infrastruct. Geotechnol.* **2014**, *1*, 83–109. [CrossRef]
23. Zarembski, A.M.; Palese, J.W.; Euston, T.L. Correlating ballast volume deficit with the development of track geometry exceptions utilizing data science algorithm. *Transp. Infrastruct. Geotechnol.* **2017**, *4*, 37–51. [CrossRef]
24. Sun, H.; Xu, Z.; Yao, L.; Zhong, R.; Du, L.; Wu, H. Tunnel monitoring and measuring system using mobile laser scanning: Design and deployment. *Remote Sens.* **2020**, *12*, 730. [CrossRef]
25. Niel, Z.; Ashiru, M.; Chen, X.; Mohamud, S.; Chen, X.; Mohamud, S.H. Appraisal of railway ballast degradation through Los Angeles abrasion, cyclic loading tests, and image technics. In *Advances in Geotechnical Engineering & Geoenvironmental Engineering; Sustainable Civil Infrastructures Series*; Springer: Berlin/Heidelberg, Germany, 2021; pp. 48–58. [CrossRef]
26. Schulte-Tiggens, J.; Förster, M.M.; Nikolovski, G.; Reke, M.; Ferrein, A.; Kaszner, D.; Matheis, D.; Walter, T. Benchmarking of various LiDAR sensors for use in self-driving vehicles in real-world environments. *Sensors* **2022**, *22*, 7146. [CrossRef]
27. Kelly, C.; Wilkinson, B.; Abd-Elrahman, A.; Cordero, O.; Lassiter, H. Accuracy assessment of low-cost LiDAR scanners: An analysis of the Velodyne HDL-32E and LiVox Mid-40's temporal stability. *Remote Sens.* **2022**, *14*, 4220. [CrossRef]
28. COPASA. Available online: <https://www.copasagroup.com/es/inicio/> (accessed on 26 December 2022).
29. Sanchis, I.V.; Franco, R.I.; Zuriaga, P.S.; Fernández, P.M. Risk of increasing temperature due to climate change on operation of the Spanish rail network. *Transp. Res. Procedia* **2020**, *45*, 5–12. [CrossRef]
30. LiVox Avia Specifications. Available online: <https://www.livoxtech.com/avia> (accessed on 29 December 2022).
31. Faro Focus 3D Specifications. Available online: [https://knowledge.faro.com/Hardware/Focus/Focus/Performance\\_Specifications\\_for\\_the\\_Focus3D](https://knowledge.faro.com/Hardware/Focus/Focus/Performance_Specifications_for_the_Focus3D) (accessed on 29 December 2022).
32. Cloud Compare. Available online: <https://www.cloudcompare.org/> (accessed on 29 December 2022).
33. González-Jorge, H.; Riveiro, B.; Armesto, J.; Arias, P. Standard artifact for the geometric verification of terrestrial laser scanning systems. *Opt. Laser Technol.* **2011**, *43*, 1249–1256. [CrossRef]
34. Besl, P.J.; McKay, N.D. A method for registration of 3-D shapes. *IEEE Trans. Pattern Anal. Mach. Intell.* **1992**, *142*, 239–256. [CrossRef]
35. Riveiro, B.; González-Jorge, H.; Martínez-Sánchez, J.; Díaz-Vilariño, L.; Arias, P. Automatic detection of zebra crossings from mobile LiDAR data. *Opt. Laser Technol.* **2015**, *70*, 63–70. [CrossRef]
36. Types of Ballast. Available online: <https://civilcrews.com/ballast-and-types-of-ballast/> (accessed on 29 December 2022).

**Disclaimer/Publisher's Note:** The statements, opinions and data contained in all publications are solely those of the individual author(s) and contributor(s) and not of MDPI and/or the editor(s). MDPI and/or the editor(s) disclaim responsibility for any injury to people or property resulting from any ideas, methods, instructions or products referred to in the content.